*Int. J. Electrochem. Sci.*, 10 **(2015)** 8284 - 8297

International Journal of
ELECTROCHEMICAL
SCIENCE
www.electrochemsci.org

# Corrosion Behavior of a Thermally Oxidized Orto-Titanium Aluminide in Synthetic Seawater

*M. Marcu*[1,*], *A. Banu*[2], *E.M. Anghel*[1], *A. Paraschiv*[3]

[1]Institute of Physical Chemistry „Ilie Murgulescu", Splaiul Independentei 202, Bucharest, Romania
[2]Politehnica University from Bucharest, Faculty of Engineering and Management of Technological System, Splaiul Independentei 313, Bucharest, Romania
[3]COMOTI- R&D Romanian Institute, Iuliu Maniu 220, Bucharest, Romania
[*]E-mail: m_marcu2000@yahoo.com

*Received:* 18 June 2015 / *Accepted:* 13 July 2015 / *Published:* 26 August 2015

Corrosion behavior of the Ti-22Al-25Nb alloy, thermally oxidized at 850 °C for 1 h, 10 h and 20 h, respectively was studied in synthetic seawater. SEM, XRD and Raman analysis confirm the presence of mostly of the rutile niobian compound, $Ti_{0.952}Nb_{0.048}O_2$ while minor phases of $AlNbO_4$, NbOx and $Al_2O_3$ are depicted in the oxidic layer developed for the oxidized samples. Potentiodynamic polarization and electrochemical impedance spectroscopy experiments performed after 72h of immersion in synthetic seawater indicated different resistance corrosions. Thus, thin oxide layer of about 1.5 µm, formed at 850 ºC for 10 h, presents the best resistance corrosion amidst investigated specimens ($i_{corr}$= 2.1 $e^{-8}Acm^{-2}$, two time smaller than untreated alloy and ten time smaller than thermally oxidized for 20h). Based on the corrosion protective ability, the untreated and thermally oxidized samples can be ranked as follows: S5 (10 h at 850 °C)>S1 (untreated)>S4 (1 h at 850 °C)>S6 (20 h at 850 °C). According to the EIS measurement results a strong capacitive response for the S5 sample, illustrated by a large phase angle which remains constant over a wide range of frequency, and a high resistance of layer which was not significantly reduced after 72 h exposure in synthetic seawater are registered.

**Keywords:** corrosion, titanium aluminides, EIS, Raman Spectroscopy

## 1. INTRODUCTION

The need for the low-density structural materials with high temperature strength and low temperature ductility for aerospace application has driven interest in titanium aluminides, especially those of the TiAlNb system [1]. Alloys of the TiAlNb system comprise a numerous group of alloys [2] including, on one hand, compounds with a low concentration of niobium (Nb) which are based

predominantly on the $\alpha_2$ (HCP) phase and, on the other hand, Nb enriched compounds based on the orthorhombic (O) phase. The O-TiAlNb phase consists mostly of the $Ti_2AlNb$ compound, i.e. the orthorhombic distorted $\alpha_2$ phase of $Ti_3A1$ [3]. Other phases present in the O-TiAlNb are $\alpha_2$ (hexagonal structure) and $\beta_0$ (based on $Ti_2AlNb$ ordered from the bcc β-phase) [4]. The alloying additives as Mo and Nb reduce the oxygen solubility and hence internal oxidation [5,6].

Titanium alloys have a strong tendency to react with oxygen, which increases formation of an adherent oxide barrier layer: this is the reason for the high corrosion resistance of these materials. However, rich niobium and titanium contents in O-TiAlNb alloy lead to formation of non-protective niobium-rich oxides such as $AlNbO_4$ as well as titania and alumina discontinuous scale [7] which limits its operation temperature between 800 °C and 900 °C. Lu et al. [8] studied the thermal oxidation of Ti-45Al-8Nb for 100 h at 900°C and the results showed that $TiO_2$ and $Al_2O_3$ were present in the metastable oxide layer even at early stages of oxidation.

Use of O-TiAlNb alloys in the civil and military flying applications with exposure to the marine environment hence their seawater corrosion is a major problem to overcome. Despite the extensive studies on developing protective oxides in order to improve titanium aluminide resistance against oxidation, there is scarce knowledge about resistance corrosion at ambient temperature in aggressive environments [9-11] e.g. seawater. Gurrappa [12] reported that Ti-13.4Al-29Nb forms protective oxide scale over its surface in marine and industrial environments at low and high temperatures.

Therefore, this study aims at evaluating the corrosion resistance of the thermally oxidized O-TiAlNb samples for different time spans, at 850 °C, in synthetic seawater by means of potentiodynamic polarization and electrochemical impedance spectroscopy (EIS). Structural investigation by SEM, X-ray and Raman spectroscopy on the untreated and oxidized specimens is due to substantiate their corrosion behavior.

## 2. EXPERIMENTAL DETAILS

### *2.1. Specimens*

**Table 1** Sample nomination according to the oxidative treatments

| Samples | Oxidative treatment |
|---|---|
| S1 | Untreated |
| S2 | Electrochemical oxidation at -0.7V/NHE |
| S3 | Electrochemical oxidation at +1V/ NHE |
| S4 | Thermal oxidized at 850 °C for 1h |
| S5 | Thermal oxidized at 850 °C for 10h |
| S6 | Thermal oxidized at 850 °C for 20h |

A Ti-Al-Nb-alloy, with chemical composition 50Ti-25Nb-22Al-1Mo-1Zr (at. %) was obtained in cast condition as main phase of orto-TiAlNb and hence denominated as base alloy (O-TiAlNb) or

S1 in Table 1. The O-TiAlNb specimens were cut into 15x10x4 mm sheets then mechanically polished and rinsed with distilled water and acetone.

### *2.2 Thermal and electrochemical oxidation*

Oxidation tests of the titanium alloy specimens were performed in a Vulcan$^{TM}$ 3-130 Ney furnace at 850 °C in air for 1 h, 10 h and 20h. Three specimens for each type underwent oxidization in these conditions to prove reproducibility of the measurements. The obtained specimens were labeled S4, S5 and S6 in Table1.

For comparative reasons electrochemical oxidation in 0.5M $Na_2SO_4$ solution for 1 hour at two different potential was performed: one at -900mV/NHE, the potential of gray- black oxide formation $NbO$-$NbO_2$ (sample S2 in table 1), and the second at + 1V/NHE, potential of white oxide formation $Nb_2O_5$ (sample S3 in table 1), according to Pourbaix diagrams [13].

### *2.3 Electrochemical measurements*

Corrosion behavior of the samples was evaluated using electrochemical measurements at room temperature in synthetic seawater with the following composition: NaCl 243.6 $gL^{-1}$; KCl 0.67 $gL^{-1}$; $CaCl_2x2H_2O$ 1.36 $gL^{-1}$; $MgSO_4x7H_2O$ 6.29 $gL^{-1}$; $MgCl_2x6H_2O$ 4.66 $gL^{-1}$; $NaHCO_3$ 0.18 $gL^{-1}$. Electrochemical measurements for each oxidation condition were carried out using a potentiostat/galvanostat PARSTAT 4000 provided with FRA module. Polarization curves were recorded from -0.5V to 1.2 V vs. Ag/AgCl with a potential scan rate of 2.5 $mVs^{-1}$ after 72 h of immersion in synthetic seawater. The experimental setup for electrochemical measurements consisted of a three-electrode glass cell with Ag/AgCl electrode as reference and a platinum foil as counter electrode. The exposed surface area of each O-TiAlNb sample was of 1.0 $cm^{-2}$. For each experimental condition, three samples were tested in order to obtain an acceptable average from these results.

Polarization curve analysis allowed us to determine the corrosion parameters corrosion potential ($\varepsilon_{corr}$) and corrosion current density ( $i_{corr}$). The EIS experiments were performed after 0.5vh and 72 h of immersion in synthetic seawater. The EIS spectra were measured at the open circuit potential in the scan frequency range of 100 kHz to 10 mHz at an amplitude of 10 mV. ZView software was used to fit the EIS data with the corresponding equivalent electric circuit. To evaluate the corrosion behavior of titanium alloys from both potentiodynamic polarization curves (CP) and electrochemical impedance spectroscopy (EIS), the CorView software was used.

### *2.4 SEM-EDS*

Before and after electrochemical testing the specimens were investigated by scanning electron microscopy (SEM) with a microscope FEI Inspect F 50 high-resolution, field emission**,** equipped with energy dispersive spectroscopy (EDS) analysis.

*2.5 XRD diffraction and Raman Spectroscopy*

X-ray diffraction (XRD) data were collected using a Rigaku Ultima IV diffractometer, with Cu Kα radiation, operating at 40 kV and 30 mA equipped with Thin Films attachment for grazing incidence X-ray measurements, at an incidence angle ω=0.5°. The XRD data were recorded at room temperature at a rate of 5° (2θ)/min over a range of 10– 70°. Rigaku's PDXL software package connected to the ICDD database was used for the phase identification.

Unpolarized solid state Raman spectra were recorded by means of a LabRam HR spectrometer (Jobin-Yvon–Horiba) over 50-2000 $cm^{-1}$ range. The 514 nm line of an $Ar^{+}$ laser was used as exciting radiation through 50× and 50 LWD objectives of an Olympus microscope in a backscattering geometry and at a confocal hole of 200 μm. The diameter of the laser spot on the sample surface amounted to < 2 μm providing a spectral resolution better than 2 $cm^{-1}$.

## 3. RESULTS AND DISCUSSIONS

*3.1. Structural characterization (SEM, Raman Spectroscopy and XRD)*

After thermal oxidation at 850 °C the O-TiAlNb sample surface changed color from white to grey black after 1-10 hours of exposure; that is different from the alpha and gamma aluminide whose color is bluish gray. This first optical analysis allows us to wait for less $Al_2O_3$ and $Nb_2O_5$ in the coating. After 20 h exposure, the color of surface starts to change from black gray to blue gray when whitish spots appear.

The surface morphologies and cross section of thermally oxidized O-TiAlNb at 850 °C for 10 and 20 h (samples S5 and S6 respectively), are shown in Figs. 1 and 2. The oxide layer thicknesses were determined to be approximately 1.5 μm and 5-6 μm for the samples S5 and S6.

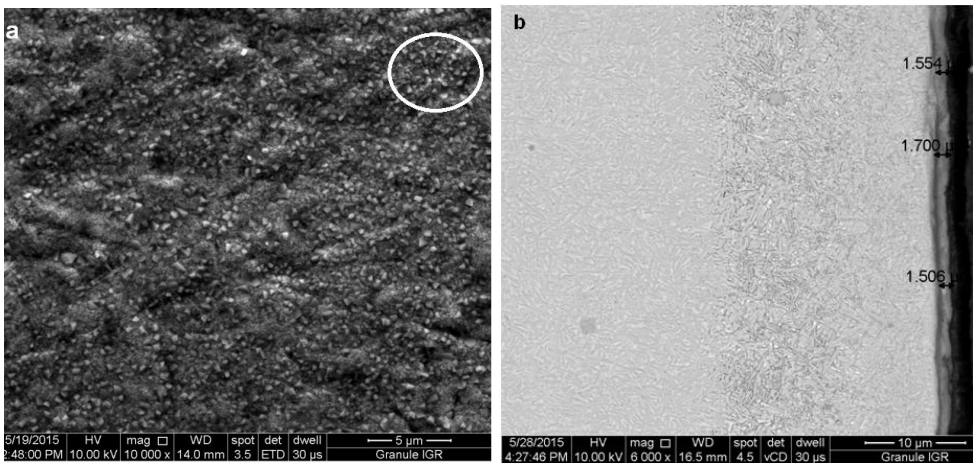


**Figure 1**. Surface morphology (a), and cross section (b) of the oxidized O-TiAlNb at 850 °C for 10 h in air atmosphere (S5).

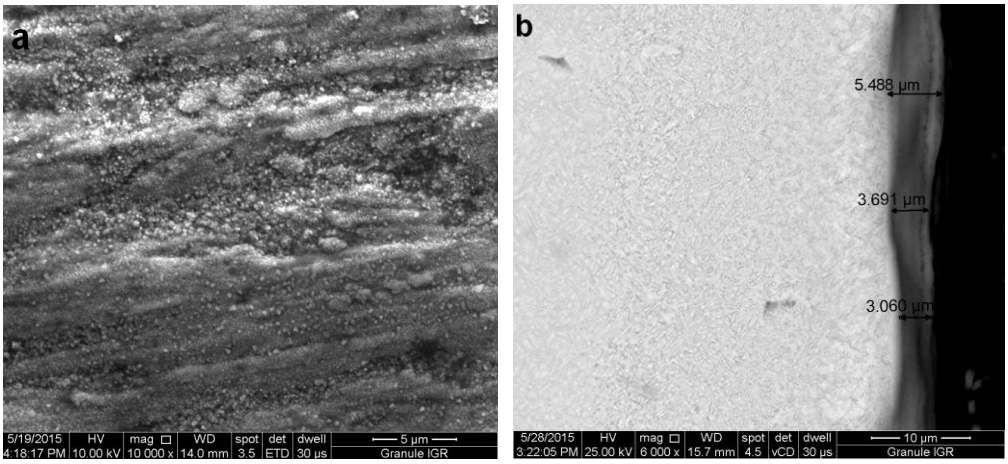


**Figure 2**. Surface morphology (a), and cross section (b) of the oxidized O-TiAlNb at 850 °C for 20 h in air atmosphere (S6).

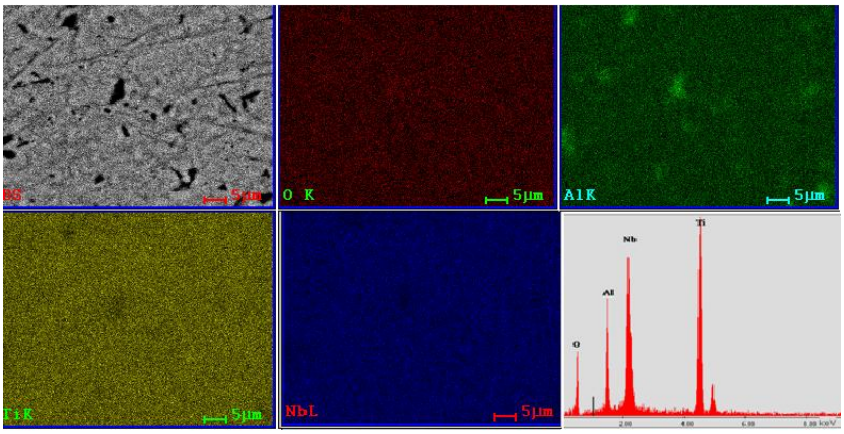


**Figure 3.** EDS map analysis of the surface oxide film formed by thermal oxidation of O-TiAlNb at 850 °C for 10 h, (S5) in selected area from Fig 1a.

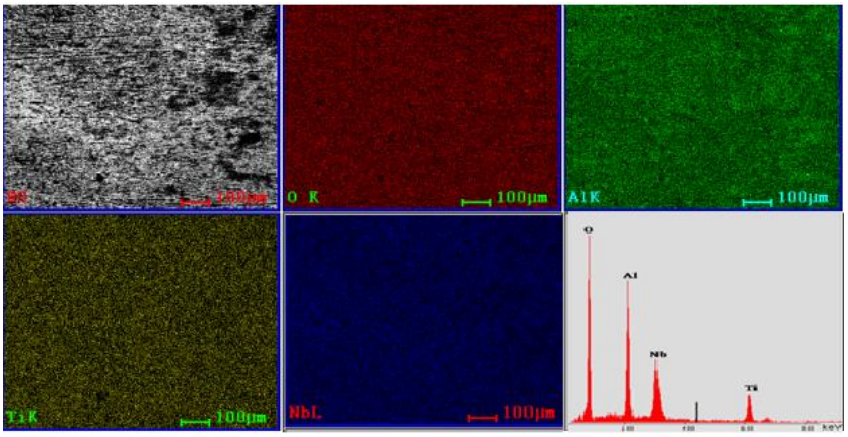


**Figure 4.** EDS map analysis of the surface oxide film formed by thermal oxidation of O-TiAlNb at 850 °C for 20 h (S6).

The maps presented in Fig. 3 and 4 show the element distribution (elemental analysis) of the surface oxide layers. Relative uniform distribution of the elements can be observed in both samples.

The bright formations in Fig. 1a, respectively dark in Fig. 3, uniformly distributed on the surfaces shows the presence of rich aluminium compounds after 10 hours of oxidation, EDS map analysis. As can be seen in Fig. 3 the surface oxygen content is small, so less oxidic compounds are formed during the initial stage of oxidation . After 20 hours of oxidation, the surface morphology can be described as covered by a blue gray colored oxide, grown layer by layer, attributed to presence of $Al_2O_3$ , NbOx species and $TiO_2$. The EDS map confirms the uniformity in element distribution, initial rich aluminum phases are less highlighted after 20 h. The surface oxygen content is higher, then we expect that the coating is formed of rich oxygen phases.

### *3.1.1 X-ray diffraction*

The XRD pattern (Fig. 5A) of the oxidized sample S6 confirms presence mainly of a niobian rutile phase ($Ti_{0.952}Nb_{0.048}O_2$) with tetragonal structure (PDF card no 01-072-7376) and a minor phase of $AlNbO_4$ (PDF card no 01-073-6074). Niobian rutile crystallites of 154.89 Å are developed on the surface of the longer exposed sample: S6.

### *3.1.2 Raman spectroscopy*

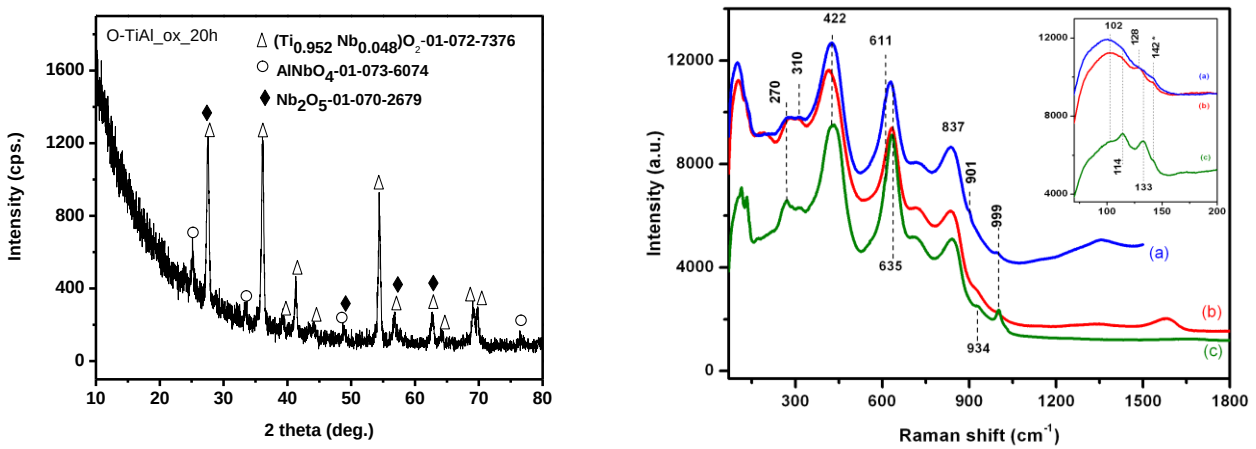


(A) (B)

**Figure 5.** X-ray pattern of the S6 sample(A), and Raman spectra (B), of the O-TiAlNb samples oxidized at 850 °C for (a) 1h, (b) 10 h, and (c) 20 h.

Raman spectra of the oxidized specimens in air at 850 °C for 1, 10 and 20 h are presented in Fig.5B. Bands within 800-1000 $cm^{-1}$ of the oxidized specimens signal the presence of $NbO_x$ surface species [14]. Analogous to low and high loadings of the niobian catalysts supported on alumina, zirconia and titania [15], bands at about 999 $cm^{-1}$ in Fig. 5B originate from Nb=O vibrations of the segregated niobia [5] on the surface of niobian rutile phase already identified by X-ray measurements.

Shifting of the 901 $cm^{-1}$ band of the sample S4 spectrum to 935 $cm^{-1}$for the longer oxidized specimens, i.e. 10 h and 20 h, respectively, points out an increasing amount of the $NbO_x$ surface species for the latter.

No Raman spectrum of the niobian rutile compound, $Ti_{0.952}Nb_{0.048}O_2$, was reported in literature. Most of the Raman bands of rutile [16] are highly overlapped with those of niobium oxides [17-19] (see Table 2). Presence of $NbO_2$ should be considered for the sample S5 due to the lack of the Raman band at about 990 $cm^{-1}$. Also, the sharp band at 418 $cm^{-1}$ of $\alpha$-$Al_2O_3$ [20] is not noticeable in Fig. 5B meaning that only transient aluminas (without Raman signals) are present.

**Table 2.** Raman modes of some oxides present in scales of oxidized O-TiAlNb alloys above 800 °C

| Compound | Raman peaks ($cm^{-1}$) | Reference |
|---|---|---|
| $TiO_2$(Rutile) | 145(w),240(m), 448(s), 613(s) and 826(w) | **14** |
| $Nb_2O_5$ | 996(s), 904(w), 848(w), 664(s), 632(s), 552(w), 472(w), 350(w), 308(m), 264(s), 240(s), and low wavenumber bands: 135(s), 124(s), 114(s), 106(s), 75(m), 56(m) | **15, 16** |
| $NbO_2$ | 92(w), 138(s), 168(s), 215(w), 246(w), doublet at 328/341(s), 400(s), 431(w), 453(w), 575(m), 622(m), 700(w), 813(m) | **18** |
| $\alpha$-$Al_2O_3$ | 378(m), 418(s), 429(w), 451(w), 576(w), 644(m) and 750(w) | **19** |

w, m and s stand for weak, medium and strong

Wider bands especially in the low wavenumber region (inset of the Fig. 5B) for the shorter time oxidized samples are a measure of smaller crystallite size.

### *3.2 Electrochemical behavior of O-TiAlNb samples in synthetic seawater*

#### *3.2.1 OCP measurements*

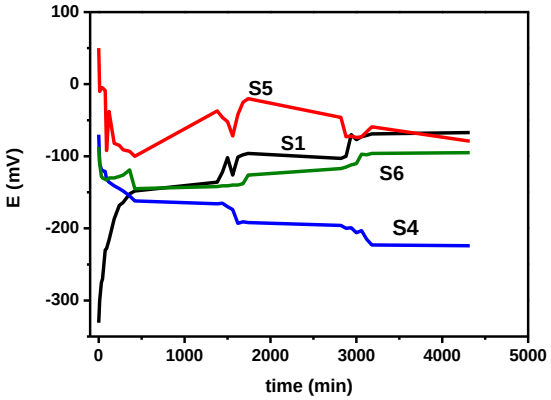


**Figure 6**. Open circuit potential vs. time for O-TiAl untreated (S1) and thermally oxidized at 850 °C (for 1h-S4; 10h-S5; 20h-S6), in synthetic seawater.

The instantaneous OCP values of samples are very different (see Fig. 6) function of surface state, untreated sample reveals the most electronegative value since the OCP of oxidized samples are with about 400 mV more positive (between -350mV and +70 mV). During immersion period, the surface state evolves and OCP values considerably change. The surface of sample S1 tends to passivate, its potential increased at about -50mV during 72 h because of oxi-hydroxide formation in aqueous environment [13].

By comparison, during an immersion time of 72 hours, the surface of short time oxidized sample S4 became more active despite of air formation of the thin oxide coating. The OCP slowly decreased from the initial value at about -70 mV up to about -200 mV. Therefore, oxidation of O-TiAlNb at 850 °C for one hour (S4) does not increase the corrosion resistance in seawater. From the OCP evolution point of view the best corrosion behavior seems to be after 10 h of oxidation, sample S5. After 20 h of thermal oxidation, sample S6, corrosion properties decrease, a behavior close to that of S1 sample.

### *3.2.2. Polarization measurements*

Fig. 7 presents the anodic polarization curves recorded over the range of -0.5 V to 1.2V for untreated and thermally oxidized O-TiAlNb samples in synthetic seawater after 72 hours of immersion. After one hour of oxidation, the corrosion potential of sample S4 shifts to electronegative values with about 60mV compared with corrosion potential of S1 and the corrosion density current increases from $4e^{-8}Acm^{-2}$ to $3e^{-7}Acm^{-2}$, which means a deterioration of corrosion resistance.

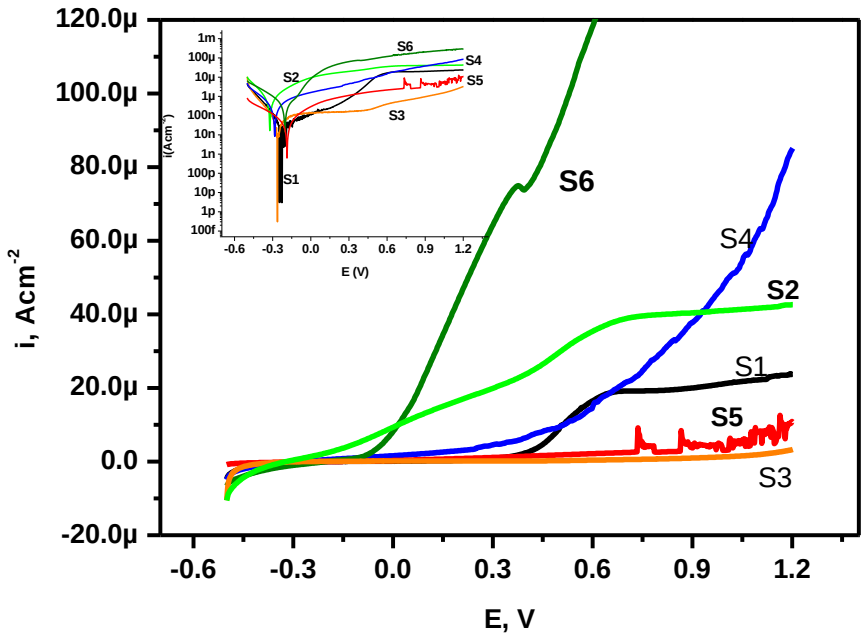


**Figure 7.** Potentiodynamic polarization curves for O-TiAlNb untreated (S1) and oxidized samples in synthetic seawater after 72 h of immersion. In set: polarization curves in logarithmic scale.

That is in agreement with the OCP evolution to the electronegative values of S4. Because of black color [21] of the surface after one hour of oxidation we consider that the formed oxide coating consists of reduced niobium oxide and/or intermetallic compounds.

The electrochemical behavior of S2 sample is slightly worse compared to the unoxidized sample S1, but superior to sample S4, one hour thermally oxidized. The electrochemical oxidation in 0,5M $Na_2SO_4$ solution for 1 hour at +1V/NHE where according with Pourbaix diagram $Nb_2O_5$ is formed, increases the corrosion resistance in seawater of O-TiAl (sample S3). From Fig. 7 it can be seen that the sample S3 is completely passive. Therefore, in the first stages of thermal oxidation, one hour in our experiment, non protective oxidic compounds at 850 °C are formed.

After 10 hours of thermal oxidation (sample S5) the corrosion potential moved towards electropositive values ($\varepsilon_{corr}$ = -187 mV) and corrosion density current slightly decrease with about 50%, ($i_{corr}$=2.1e$^{-8}$ Acm$^{-2}$). The electrochemical behavior of S5 sample is similar to that of S3 sample electrochemically oxidized at +1V/NHE, where according to literature [22], $Al_2O_3$, $TiO_2$ and $Nb_2O_5$ as protective phases are formed. According to information from literature [22-24], during electrochemical oxidation of O-TiAlNb alloy, a thin and complex oxidic film of Nb and Al in $TiO_2$ matrix covers the surface. Therefore, this explains the similar behavior between S5 and S3 samples.

Increasing in oxidation time up to 20 hours (S6) does not improve the corrosion resistance despite the increase of coating thickness. As is showed in the Fig. 7 the corrosion current density of S6 sample is about 3.05e$^{-7}$Acm$^{-2}$, seven times higher than corrosion current density of the untreated sample. The composition of oxide coating is quite different from those formed after 10 hours of exposure according to spectral and SEM analysis. The difference consists in formation of AlNbO4, less resistant from the corrosion point of view. SEM images show an uniform coating formed during 10 hours of exposure at 850 ºC, and very small aluminum-rich phases uniformly distributed (see Fig 3). The thin oxide layer formed at 850 ºC for 10 h is more compact and protective against corrosion than the one formed at 850 ºC for 20 h.

### *3.2.3. Electrochemical impedance spectroscopy measurements*

To evaluate the stability of the oxide films formed over time, electrochemical impedance spectroscopy testing was performed on samples untreated and thermally oxidized at 850 °C in seawater solution. The Nyquist plots acquired at early stages and after 72 hours of immersion in synthetic seawater are shown in Fig.8. At early time of immersion, the thermally oxidized specimens show a different behavior. The untreated specimen (S1) exhibits only a single semicircle followed by a Warburg diffusion tail for the specimen oxidized for a short time (S4). The specimens oxidized for longer time exposure (S5 and S6) exhibit the high semicircle in the high frequency range, followed by a loop in the low frequency region (S6). The high-frequency loop might be due to oxide layer defects, while the low-frequency loop is a measure of the corrosion process [25]. The diameter of the semicircle is higher for the oxidized specimens compared with untreated specimen and changes in time. These changes suggest a dependence on the nature and thickness of the oxide layer.

In order to get a better insight about the mechanism, Bode impedance and Bode phase angle were performed. According to the Bode plots diagram presented in Fig. 8(b, d, e, f) a highly capacitive behavior, typical for passive materials, is indicated from medium to low frequencies by phase angles approaching -80°, suggesting that a highly stable film is formed on S1 and S4 samples in the seawater. The oxidized samples S5 and S6 exhibited a strong capacitive response illustrated by a large phase angle close to -50°, which remained constant over a wide range of frequency (100 kHz to 10Hz for S6 and over whole frequency range for S5). The large phase angle peak is typical of passive surfaces, which indicates a near capacitive behavior.

Three different equivalent electric circuit models (C1-C3) presented in Fig. 9 can fit the EIS data. The equivalent circuit proposed for the untreated sample S1, closely simulates the formation of a compact film with a polarization resistance R1 and a capacitance CPE1, similar to the one used by Pan et al. [25]. In case of S4 oxidized sample at 850 °C for one hour, the EIS plots are characterized by two time constants and circuit equivalent model simulates the oxide layer grown on the passive film surface. In this circuit, R1 and R2 represent the resistance of the oxide layer and passive film of O-TiAl substrate, and CPE1 and CPE2 designate the capacitances of the oxide layer and the passive film. Several papers have also used a similar model to explain the corrosion behavior of titanium alloys in NaCl and Ringers's solution, respectively [10,26,27].

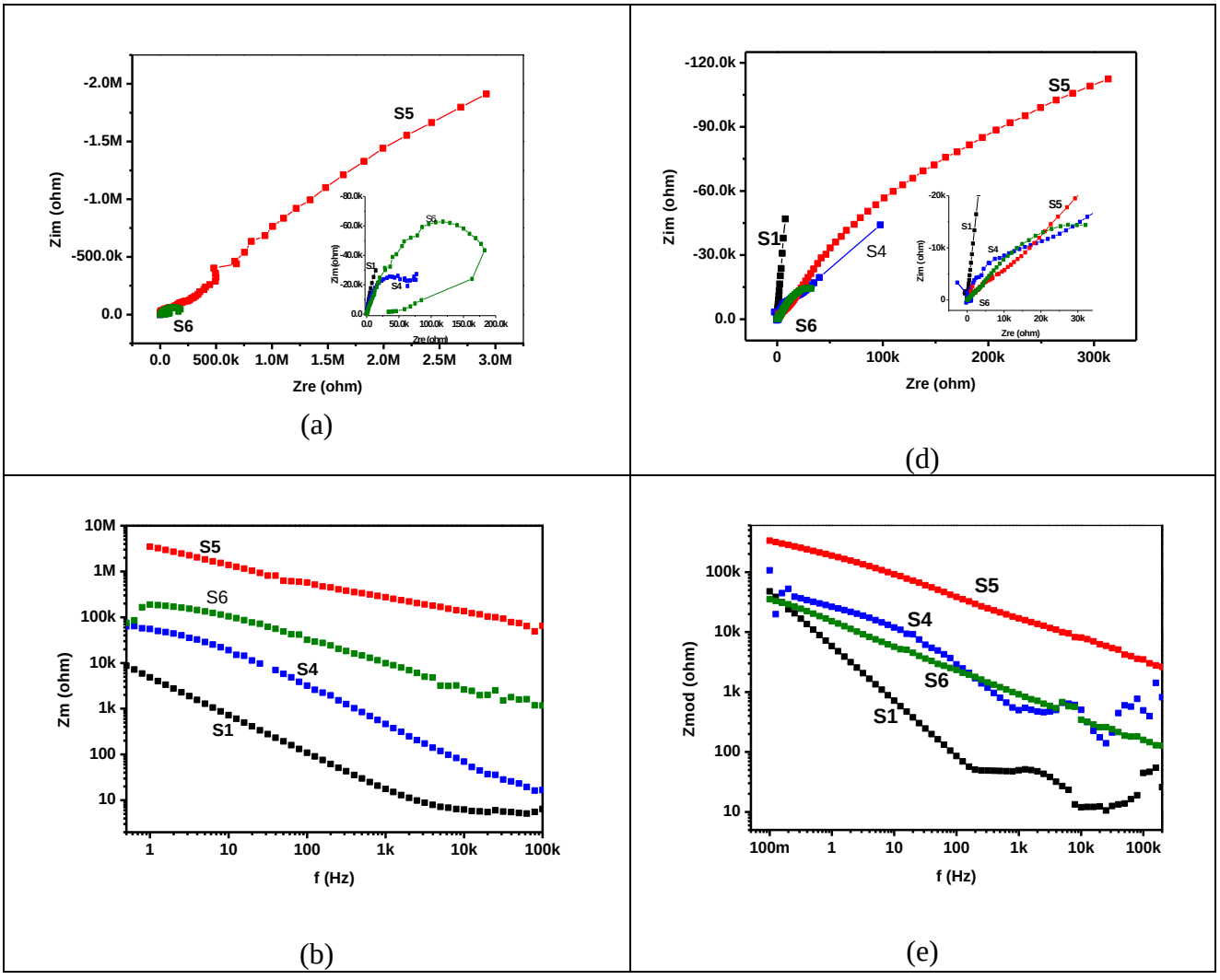

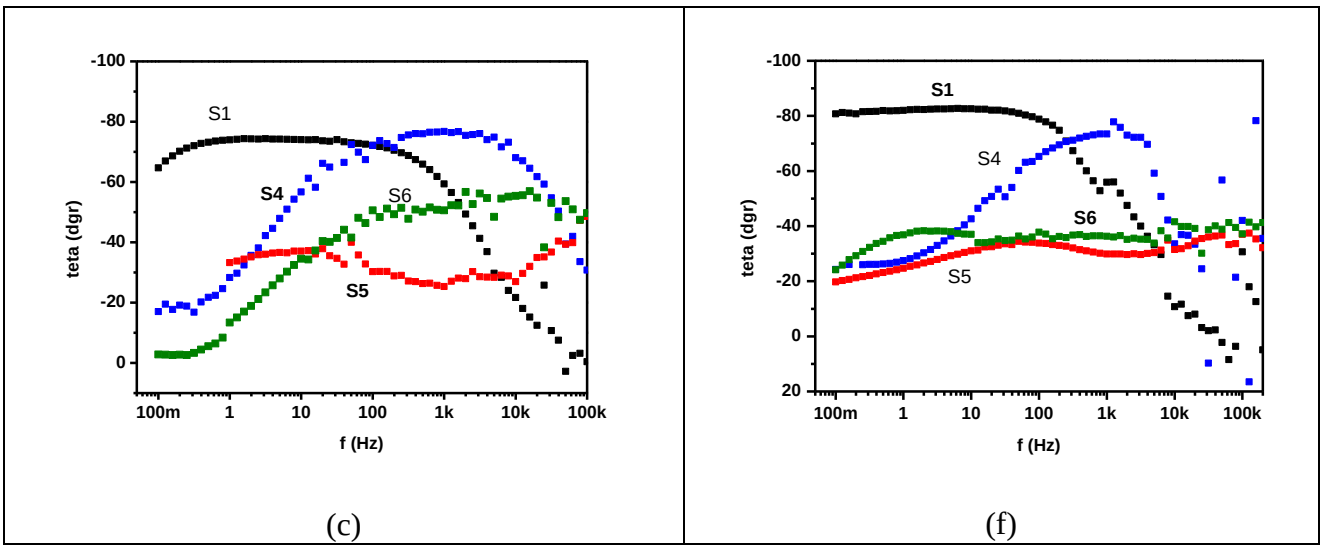


**Figure 8.** EIS plots obtained for O-TiAlNb samples untreated (S1) and thermally oxidized at 850 °C (for 1h-S4; 10h-S5; 20h-S6) in synthetic seawater for two exposure times: t=0 (a, b, c) and t=72 h (d, e, f). Inset: detail for Nyquist plots in the range of high frequency.

For a longer exposure time of oxidation at 850 °C, the EIS plots are very different. The equivalent circuit models proposed for S5 and S6 samples closely simulate the oxide layer formed on the surface of O-TiAl followed by Warburg diffusion. The resistance of the oxide layer is higher for S5 than S6 sample, although during oxidation it is lower.

The EIS parameters as determined by fitting the EIS data using Zview software are listed in Table 3. The good agreement between the experimental data and fitted data is confirmed by the $\chi 2$ values of about $10^{-3}$.

By comparing the results of EIS parameters presented in Table 3 for S6 with S5 sample, it can be seen a great difference for the Warburg element, which is an indicative of easier diffusion of electrolyte through the pores of the oxide film.

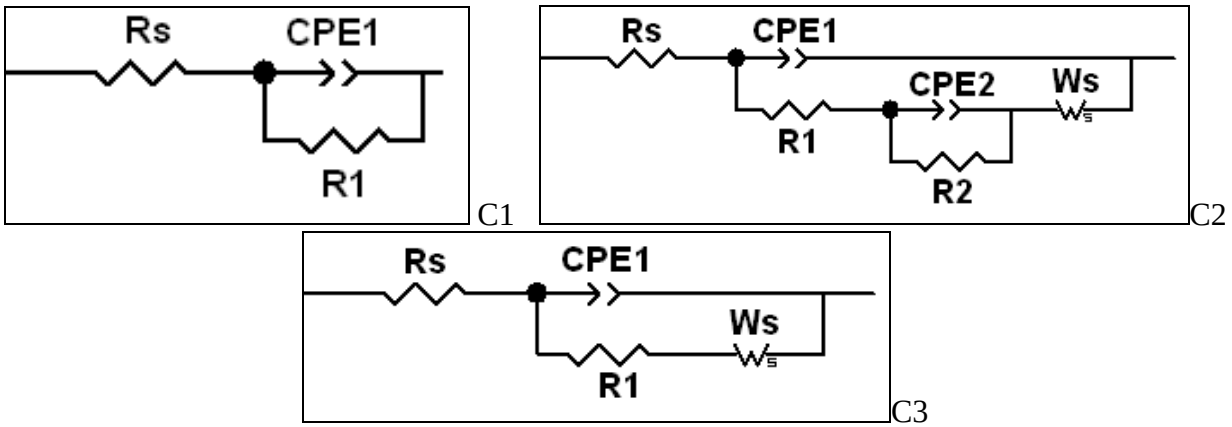


**Figure 9.** The equivalent circuits for EIS of the untreated (C1) and thermally oxidized specimens (1h-C2; 10h and20h-C3) in synthetic seawater after 72 h of immersion.

**Table 3.** Fitted results from EIS plots obtained for untreated and thermally oxidized samples after 72 h of immersion in synthetic seawater

| Sample | Circuit model | Rs ($\Omega cm^{-2}$) | CPE-1 ($S \cdot s^n cm^{-2}$) | n1 | R1 ($\Omega$) | R2 ($\Omega$) | W-R ($\Omega cm^{-2}$) | CPE-2 ($S \cdot s^n cm^{-2}$) | n2 | $\chi 2$ |
|---|---|---|---|---|---|---|---|---|---|---|
| S1 | C1 | 14.3 | $1.15e^{-6}$ | 0.86 | $3.5e^{4}$ | - | - | - | - | 0.009 |
| S4 | C2 | 12.3 | $1.2e^{-7}$ | 0.86 | 0.3 | $2.7e^{4}$ | $1.2e^{5}$ | $6.1e^{-8}$ | 0.75 | 0.006 |
| S5 | C3 | 13.5 | $7.7\ e^{-10}$ | 0.89 | $3.5e^{6}$ | - | $2.5e^{6}$ | - | - | 0.009 |
| S6 | C3 | 318 | $1.2e^{-8}$ | 0.88 | 54 | - | $4.4e^{2}$ | - | - | 0.009 |

The occurrence of a Warburg diffusion tail in the low frequency region of the Nyquist plot of sample S6 indicates the fact that the corrosion process is controlled by diffusion. Decreased resistance after 72 hours of immersion in seawater for sample S6 could be due to the oxide porous layer. The surface morphology of the oxide layer presented in Fig. 2 confirms the high roughness of the layer as well as its unevenness.

An important factor from the corrosion resistance perspective is the charge transfer resistance which controls the electrochemical process rate at the metal/electrolyte interface. The higher resistance, R1, and lower capacitance for sample S5 oxidized at 850 °C for 10 hours suggest a better corrosion resistance than untreated samples. The R2 and CPE2 values for sample S4 oxidized at 850 °C for one hour imply slightly better corrosion resistance than the untreated sample S1. Based on the spectral analysis (bigger crystallite size with segregation phase of the niobium oxide on the surface oxide layer) and porous oxide layer for sample oxidized at 850 °C for 20 hours (S6) are probable the reasons for the lower resistance corrosion in seawater.

## 4. CONCLUSIONS

The corrosion resistance of untreated and thermally oxidized (at 850 °C for 1, 10 and 20 h) O-TiAlNb samples in synthetic seawater was studied by potentiodynamic polarization and EIS techniques in order to assess the corrosion protection in marine environmental. The relevant conclusions are summarized as following:

1. XRD and Raman spectra confirm the presence of mainly a niobian rutile phase ($Ti_{0.952}Nb_{0.048}O_2$) with minor phases of $AlNbO_4$ and of $NbO_x$ surface species for sample S4. For samples S5 and S6 the spectral measurements reveal the formation of the niobian rutile along with $NbO_2$ and $Al_2O_3$ in $TiO_2$ matrix.

2. The surface morphology of the thermally oxidized samples discloses lower surface oxygen content, so that non-protective oxidic compounds are formed in the initial stage of oxidation (one hour). After 10 and 20 hours of oxidation, the surface morphology can be described as covered by a thicker coating, grown layer by layer, with thickness between 1.5 to 5.6 μm. The thin oxide layer formed at 850 ºC for 10 h is more compact and protective against corrosion than the oxide layer formed at 850 ºC for 20 h.

3. Nobler OCP, lower corrosion current density, R1 and C1 values of S5 sample, show a dependence on the nature and thickness of the surface layer. The thin oxide layer of about 1.5μm, formed at 850 ºC for 10 h, presents a better resistance corrosion ($i_{corr}$= 2.1 $e^{-8}$Acm$^{-2}$, i.e. two and ten times smaller than those of untreated and respectively thermally oxidized for 20 h alloy).

Based on the corrosion protective ability, the untreated and thermally oxidized samples can be ranked as follows: S5(10h at 850 °C)>S1(untreated)>S4(1h at 850 °C)>S6(20h at 850 °C).

4. From the EIS measurements results a strong capacitive response for S5 sample, illustrated by a large phase angle close to -50°, which remains constant over whole frequency range (100 kHz to 1Hz).

From corrosion point of view, the thermal oxidation at 850 °C for short time (10 h) is a promising surface treatment for O-TiAlNb which is exposed to a marine environment.

ACKNOWLEDGEMENT
This work was funded by National Project PCCA contract nr. 65/2012. Also, the financial support of EU (ERDF) INFRANANOCHEM – Nr. 19/01.03.2009 project was gratefully acknowledged.

**References**

1. L.A. Bendersky, W.J. Boettinger, F.S. Biancaniello, *Mater. Science and Eng., A, 152 (1992) 41*
2. D. Banerjee, A.K. Gogia, T.K. Nandy et al. *The Physical Metallurgy of Ti3Al based Alloys*, Structural Intermetallics, Warrendale (PA): TMS-AIME, (1993)
3. D. Banerjee, A.K. Gogia, T.K. Nandy, V.A. Joshi, *Acta Metall*., A36 (1988) 871
4. K. Muraleedharan, T.K. Nandy, D. Banerjee, S. Lele, *Intermetallics*, 3 (1995) 187
5. Y. Shida and H. Anada, *Metall. Mater. Trans. A*, 35 (1994) 623
6. T.K. Roy, R. Balasubramaniam, A. Ghosh, *Metall. Mater. Trans. A*, 27 (1996) 3993
7. C. Leyens, M. Peters, *Titanium and Titanium Alloys: Fundamentals and applications*, Wiley-VCH Verlag GmbH, Wenheim, (2003)
8. W. Lu, C.I. Chen, L.L. He, F.H. Wang, J.P. Lin, G.L. Chen, *Corros. Sci*., 50 (2008) 978
9. Y. Song, X. Zhu, X. Wang, J.Che, Y. Du, *J. Appl. Electrochem*., 31 (2001) 1273
10. E. Saebnoori, T. Shahrabi, H. Jafarian, M. Ghaffari, *Res. Chem. Intermed*, 41 (2015) 1079
11. C. Delgado-Alvarado, P.A. Sundaram, *Corros. Sci*. 49 (2007), 3732
12. I. Gurrappa, *Intermettalics*, 11 (2003) 867
13. M. Pourbaix, *Atlas of equilibrium Atlas of Electrochemical Equilibria in Aqueous Solutions*, NACE International, Cebelcor, (1974)
14. E. Uyanga, A. Gibaud, P. Daniel, D. Sangaa, G. Sevjidsuren, P. Altantsog, T. Beuvier, C. Hao Lee and A.M. Balagurov, *Mat. Res. Bull*, 60 (2014) 222
15. L.J. Burcham, J. Datka, I.E. Wachs, *J. Phys. Chem., B* 103 (1999) 6015
16. O. Frank, M. Zukalova, B. Laskova, J. Kurti, J. Koltai and L. Kavan, Phys. *Chem. Chem. Phys*., 14 (2012) 14567
17. B.X. Huang, K. Wang, J.S. Church, Y.S.W. Li, *Electrochim. Acta*, 44 (1999) 2571
18. P. S. Dobal, A. Dixit, R. S. Katiyar, H. Choosuwan, R. Guo and A. S. Bhalla**,** *J. Raman Spectrosc.*, 33 (2002) 121
19. S. Lee, H. Yoon, I. Yoon and B. Kim, *Bull. Korean Chem. Soc*., 33 (2012) 839
20. J.A. Xu, E. Huang, J.F. Lin, and L. Y. Xu, *Am. Mineral*, 80 (1995) 1157
21. 21. P. Hirtopanu, R. J. Fairhurst, G. Jakab *Proc. Rom. Acad., Series B*, 17 (2015) 45
22. I. Milosev, T. Kosec, H.H. Strehblow, *Electrochim. Acta*, 53 (2008) 3547
23. Z. P. Yao, Z.H. Jiang, S.G. Sim, X.T. Sun, X.H. Wu, *Electrochim. Acta*, 50 (2005) 3273

24. C. Vasilescu, P. Drob, E. Vasilescu, P. Osiceanu, S. I. Drob , M.V. Popa, *Int. J. Electrochem. Sci*., 8 (2013) 10733
25. J. Pan, D.Thierry, C. Leygraf, *Electrochim. Acta*, 41 (1996) 1143
26. P.B. Zang, B. I. Wang, I. Li, Y.F. Zheng, *Dent. Mater.*, 27 (2011) 214
27. L. Wu, J. Liu , M.Yu, S.Li, H. Liang, M. Zhu, *Int. J. Electrochem. Sci*., 9 (2014) 5012